Journal of Power Sources 187 (2009) 148–155

Contents lists available at ScienceDirect

Journal of Power Sources

journal homepage: www.elsevier.com/locate/jpowsour

Improved fuel use efficiency in microchannel direct methanol fuel cells using a hydrophilic macroporous layer

Ai Kamitani [a], Satoshi Morishita [a], Hiroshi Kotaki [a], Steve Arscott [b,*]

[a] Advanced Technology Research Laboratories, Corporate Research and Development Group, SHARP Corporation, 2613-1 Ichinomoto-cho, Tenri, Nara 632-8567, Japan
[b] Institut d'Electronique, de Microélectronique et de Nanotechnologie (IEMN), CNRS UMR8520, University of Lille, Avenue Poincaré, Cite Scientifique, Villeneuve d'Ascq 59652, France

ARTICLE INFO

Article history:
Received 23 May 2008
Received in revised form
23 September 2008
Accepted 19 October 2008
Available online 5 November 2008

Keywords:
Micro-direct methanol fuel cell
Silicon microsystems
MEMS
Macroporous materials

ABSTRACT

We demonstrate state-of-the-art room temperature operation of silicon microchannel-based micro-direct methanol fuel cells (μDMFC) having a very high fuel use efficiency of 75.4% operating at an output power density of 9.25 mW cm^{-2} for an input fuel (3 M aqueous methanol solution) flow rate as low as 0.55 μL min^{-1}. In addition, an output power density of 12.7 mW cm^{-2} has been observed for a fuel flow rate of 2.76 μL min^{-1}. These results were obtained via the insertion of novel hydrophilic macroporous layer between the standard hydrophobic carbon gas diffusion layer (GDL) and the anode catalyst layer of a μDMFC; the hydrophilic macroporous layer acts to improve mass transport, as a wicking layer for the fuel, enhancing fuel supply to the anode at low flow rates. The results were obtained with the fuel being supplied to the anode catalyst layer via a network of microscopic microchannels etched in a silicon wafer.

1. Introduction

Microtechnology is enabling the miniaturization of methanol fuel cells into compact micro-direct methanol fuel cells (μDMFC) [1–5]. Fully optimized μDMFCs would have a large impact for powering a wealth of portable electronic good now available to the consumer; the potential market is quite simply huge. μDMFCs have potentially a high energy density and can hence supply power in the milliwatt range for a long time. In addition, refueling time is rapid, quasi-instantaneous, compared to the several hours recharge time for lithium-ion type batteries. On the other hand, current μDMFC prototype systems suffer from mass transport issues [6–13]; we address here fuel supply mass transport at the anode of a miniaturized μDMFC by the modification of the diffusion layer stack via the insertion of a novel hydrophilic macroporous layer which is believed to equalize the fuel concentration over the whole anode catalyst cell area and aid carbon dioxide bubble removal at low fuel flow rates.

2. Experimental

Our basic set-up used to perform the fuel cell measurements (with and without the macroporous layer) is shown in Fig. 1. Porous gas diffusion layers (GDL) carbon-based sheets GDL-24BC and LT-1400 were obtained from (ETEK, USA) and (SGL Carbon, Germany) and were used for the fuel and air diffusion layers, respectively, a gold mesh (Goodfellow, UK) as electrodes and a membrane electrode assembly (MEA) composed of a three layer MEA3 optimized Nafion® 117 PFSA (DuPont, USA) having a Pt–Ru anode. These elements were stacked between two 3-in. silicon wafers (Siltronix, France) which had pre-etched microscopic microchannels on their surface to supply fuel and air to the anode and cathode, respectively. The silicon wafers, diffusion layers, macroporous layers, spacer layers, electrodes and Nafion®117-based PEM were in turn stacked and held together by two rigid acrylic glass plates (thickness = 0.5 cm) held together by screws to regulate the pressure. Spacer layers were stacked according to macroporous layer thickness. A micrometer was used to ensure uniformity and regulate thicknesses, e.g. the macroporous layer thickness. The system contained thru-holes to enable connections with the Nanoport™ connectors. Polydimethylsiloxane (PDMS) layers (0.5 mm) were employed between the acrylic glass plates and the silicon wafers to prevent possible wafer cleaving. Standard silicon-based microtechnology was employed to fabricate the microchannels in the anode and cathode silicon wafers. Photolithography and deep reactive ion etching (DRIE) techniques (Surface Technology Systems, UK) were optimized to etch microchannels silicon wafers. For the anode a single serpentine shaped microchannel was designed to supply the fuel. The channel width was 100 μm and channel height 100 μm whilst the total channel length was 8 cm running over

* Corresponding author. Tel.: +33 320197948.
E-mail address: steve.arscott@iemn.univ-lille1.fr (S. Arscott).

0378-7753/$ – see front matter © 2008 Elsevier B.V. All rights reserved.
doi:10.1016/j.jpowsour.2008.10.085

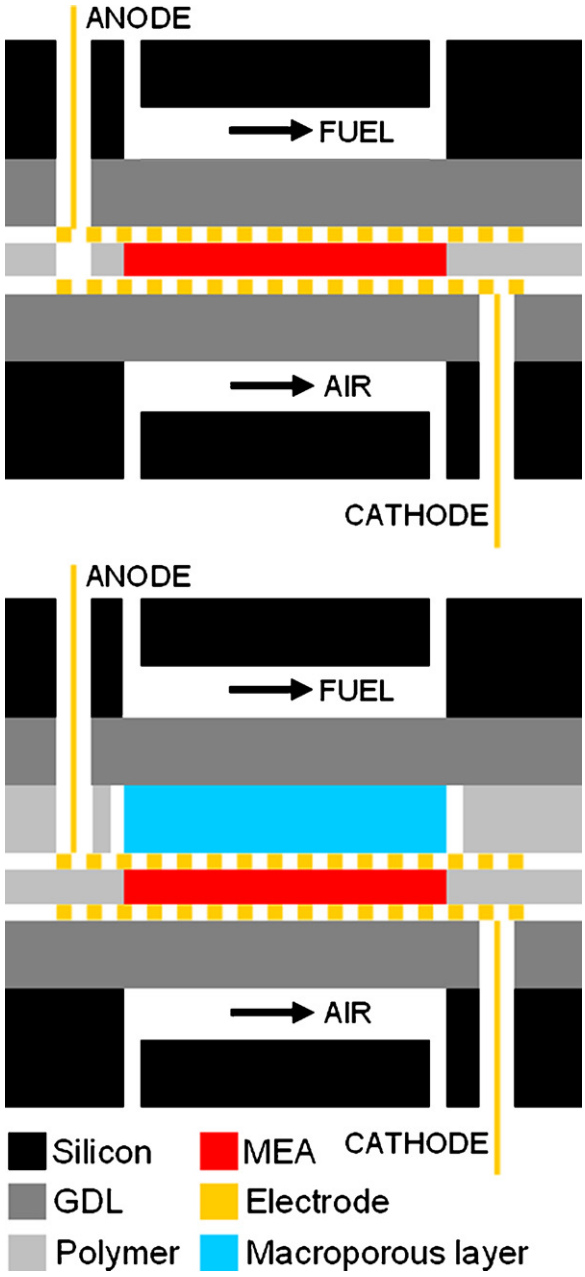

Fig. 1. Micro-DMFC experimental set-up. (a) With and (b) without macroporous layer showing the silicon wafer (black), the gas diffusion layers (dark grey), a polymeric spacer layer, the MEA (red), the electrodes (gold) and the macroporous layer (blue). (For interpretation of the references to color in this figure legend, the reader is referred to the web version of the article.)

an active cell surface of 0.25 cm^2. The interior microchannel surface contained in the active fuel cell area was made hydrophilic by masking techniques during the rendering of the silicon wafer surface hydrophobic via a plasma deposition of a fluorocarbon layer (~1 μm). The fuel solution (3 M CH_3OH:H_20) and the oxidant air (21% O_2) are introduced via thru-holes pierced by DRIE in each Si wafer which directly join the microchannels on the opposite wafer side to provide microfluidic and gas flow inputs and outputs. The fuel cell had an effective anode catalyst surface of 0.5 cm by 0.5 cm (0.25 cm^2); the catalysis area is located underneath the single serpentine microchannel area through the fuel diffusion layer and collector electrode. For the cathode, four serpentine shaped microchannels for air were arranged in parallel; the microchannels had a width of 200 μm and a height of 150 μm with a total length of 4 cm, the microchannel surface and the wafer surface was rendered hydrophobic via a plasma deposition of a fluorocarbon thin film (~1 μm). A high precision tubing pump and a mass flow controller were employed to control the fuel mixture flow and air flow, which were connected to the fuel and air inlets on the Si wafers with microchannels. Electrical and microfluidic circuits were implemented for the fuel cell measurements. The standard electrical circuit used for fuel cell measurements employed a current source (0–50 mA) and 3441 A digital multi-meters (Agilent, USA). The tips of probes were carefully brought into contact with the gold mesh sheet collector electrodes. The microfluidic circuits employed plastic tubing (OD = 1587 μm; ID = 762 μm) supplied from (Cluzeau, France) which was connected to the Nanoports™ on the fuel and air-side of the silicon wafers. The fuel flow rate was controlled by an IPC4 high precision multi-channel dispenser peristaltic pump (Ismatec, Switzerland) having a mass flow range of 0–39 μL min^{-1} and an STEC SEC-7300 mass flow controller (Horiba, Japan) was employed for the air having a mass flow range from 2 to 50 sccm.

3. Results and discussions

Measurements were conducted in the following sequence: (i) initial reference measurements without a macroporous layer and (ii) measurements using various macroporous layers. All measurements were taken at room temperature (~300 K); the output power density (mW cm^{-2}) is plotted as a function of current density (mA cm^{-2}) and was evaluated from the measured current (mA) versus voltage (mV) characteristics. Finally, the subsequent fuel use efficiency φ (%) of the fuel cell was evaluated at a given fuel flow rate (mol s^{-1}). The fuel use efficiency of the cell is calculated from the current density at the maximum output power, the fuel flow rate, the fuel concentration and the cell area. It should be noted that great care was taken to repeat the measurements several times; repeated *I–V* measurements were taken for a given microfluidic test set-up and also following dismantling and reassembling the microfluidic set-up to further ensure repeatability of the electrical results; this is very important as variations in set-up can cause leaks in the microfluidic/gas circuit which can lead to erroneous measurements thus causing incorrect conclusions to be drawn.

The results of the initial reference measurements without the inclusion of the macroporous layer [see Fig. 1 for set-up] are shown in Fig. 2; (a) shows output voltage as a function of applied current, and (b) shows power density versus current density. A maximum output power of 8 mW cm^{-2} was observed for a fuel flow rate of 2.76 μL min^{-1}. Following this, a single macroporous layer (A = 0.25 cm^2) was inserted between the standard anode diffusion layer and anode collector electrode. A total of five macroporous layer candidate materials (A–E) have been investigated in this study. By carefully selecting various fibrous materials, we were able to experiment into the effect of layer porosity, hydrophobicity and layer thickness. Scanning electron microscopy (SEM) images of the five fibrous materials used in this study, plus the standard hydrophobic anode diffusion layer (GDL-24) which was used throughout, are shown in Fig. 3. Macroporous layer A is actually a combination of two fibrous layers; one surface layer (see Fig. 3(a)) consisting of polyester fibers and polypropylene fibers whose surface (<10 μm thick) is hydrophobic (wetting contact angle θ_c for 3 M methanol solution was measured to be 120° ± 5 using a wetting contact angle meter supplied by DigiDrop, France); incidentally, the wetting contact angle the fuel makes with the GDL-24 diffusion layer was determined to be 134° and 107° after multi-use via the same technique. The other side, which made up the volume of macroporous layer A, is shown in Fig. 3(a, inset)

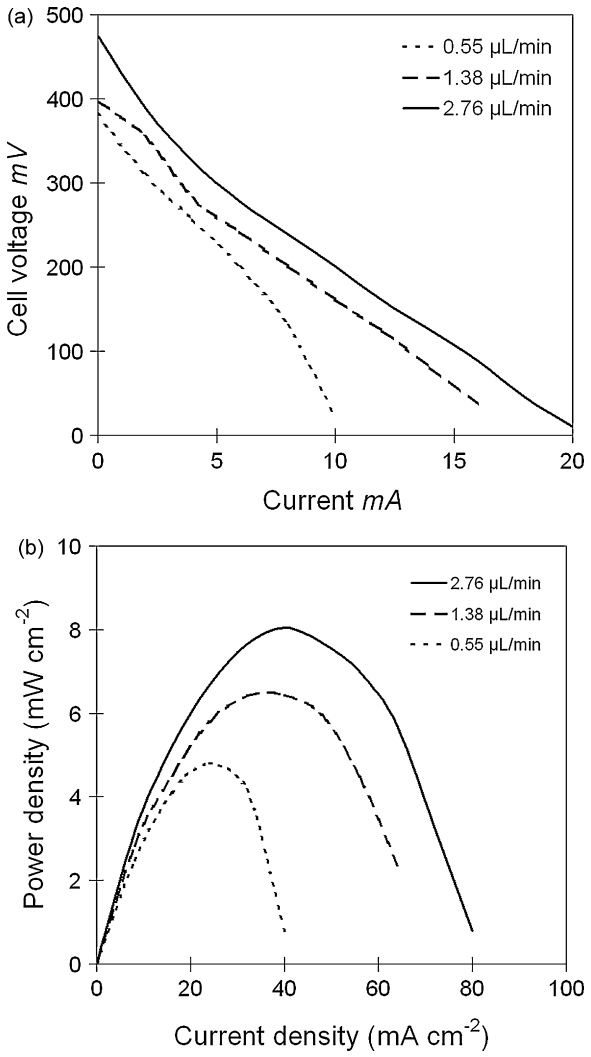

Fig. 2. Standard reference electrical measurements of the micro-DMFC prior to the insertion of the macroporous layers: (a) voltage–current and (b) output power–current density as a function of input fuel flow rate at a constant air-flow rate of 30 sccm to the cathode.

and consists of cellulose-based fibers which have an ultra absorption property (having a hydrophilic surface; $\theta_c < 10^\circ$). The fibers on the hydrophilic side have a specific shape which radiate locally from central point to promote liquid spreading in the plane of the sheet. Macroporous layer B (Fig. 3(b)) is a very low porosity fibrous paper which is commonly used for testing perfume and macroporous layer C shown in Fig. 3(c) is a cotton-based fibrous material. Macroporous layers D and E are both relatively hydrophobic glass fiber-based papers having low (D) and high (E) porosity (Fig. 3(d) and (e)). The SEM image for diffusion layer (GDL-24) is Fig. 3(f).

The fuel cell power output performances were measured with different macroporous layers present; the *V–I* and *P–J* results are shown in Fig. 4. All measurements were conducted at a constant input fuel flow rate of 2.76 µL min^{-1} and an air flow rate of 30 sccm; a high air flow rate was chosen at the cathode to avoid mass transport problems and enable us to observe the effect of changing the anode conditions. It is clear from Fig. 4(b) that the insertion of two macroporous layers A [in configuration 1 = A1, i.e. the hydrophilic surface in contact with the anode catalyst layer] and C improves cell performance (in terms of maximum power output) compared to the reference measurements without the macroporous layer whilst the insertion of two macroporous layers (B and E) reduces the cell performance; the maximum output power with macroporous D remains approximately the same. In terms of thickness, macroporous layer layers A and D have approximately equal thicknesses, namely 480 ± 10 µm and 460 ± 10 µm experiments were able to show that there is a correlation between the properties of the inserted macroporous layer and the power output of the fuel cell as layers A and C gave the best results (9.9 mW cm^{-2} at 2.76 µL min^{-1} with macroporous layer A in configuration A1) and layer D gave result similar to having no macroporous layer inserted (8.6 mW cm^{-2} at 2.76 µL min^{-1}).

In order to interpret the results we characterized the macroporous layers; in terms of wetting contact angle, a contact angle meter (EWS, France) can be used to characterize the hydrophilic/hydrophobic nature of the macroporous layer. Contact angle measurements were repeated several times to ensure reproducibility of ±5°. In terms of porosity, the SEM images can be used to rank the macroporous layers in terms of pore size. It can be seen from the SEM images that a precise value of the pore diameter is difficult to extract, however, observations enable us to estimate the pore size in terms of $d_p < 10$ µm, 10 µm < d_p < 50 µm and $d_p > 50$ µm. In addition to this we can use absorption measurements to estimate the absorption ratio and the liquid/solid volume ratio. The absorption ratio is defined as the ratio of the wet macroporous layer weight against the dry weight. The liquid/solid volume ratio, i.e. the ratio of the available liquid volume in the macroporous layer V_l over the total volume of the macroporous layer V_t, of the layers was estimated using the volume/density method; wetting, weighing and drying was repeated a several times after excess fluid removal giving a measurement reproducibility of ±10%. Table 1 shows the measured thickness of the macroporous layers, the absorption ratio, the measured liquid/solid volume ratio and the wetting contact angle of the fuel (3 M aqueous methanol solution) on the macroporous layer surface.

If we rank the macroporous layers in terms of most hydrophilic to most hydrophobic then we have: A1, B, C, D and E. If we now rank the macroporous layers in terms of pore size d_p from the most porous to the least porous we have: E, A, C, D and B. In terms of the absorption ratio and liquid/solid volume ratio ranking we have A, C, E, D, B and A, C, D, E and B, respectively. Combining these observations with those of the fuel cell performances we can clearly conclude that enhanced performance is brought about by the use of a highly hydrophilic macroporous layer having a relatively high porosity $d_p > 50$ µm confirmed by a high liquid/solid volume ratio. Interestingly, macroporous layer D has comparable properties (pore size and hydrophobicity) to the standard GDL used in the experiment and leads to a similar performance as the reference performance. It is important to note that the absorption results given in Table 1 be defined as *ex situ*; when the various macroporous layers are being used in the experiment, i.e. *in situ*, they could be compressed and their absorbency properties could vary from those presented in Table 1. However, with reference to Fig. 1(b) we assume that the inclusion of the polymeric spacer

Table 1
Measured properties of the macroporous layers A–E used in the experiments.

Layer	Thickness (µm)	Absorption ratio	Liquid/solid volume ratio	Contact angle, θ_c
A	480	5.3	0.87	<10° (120° ± 5)[a]
B	380	0.9	0.29	<10°
C	1400	3.3	0.68	<10°
D	460	1.9	0.48	115° ± 5
E	250	2.9	0.36	120° ± 5

[a] Contact angle measured on hydrophobic surface.

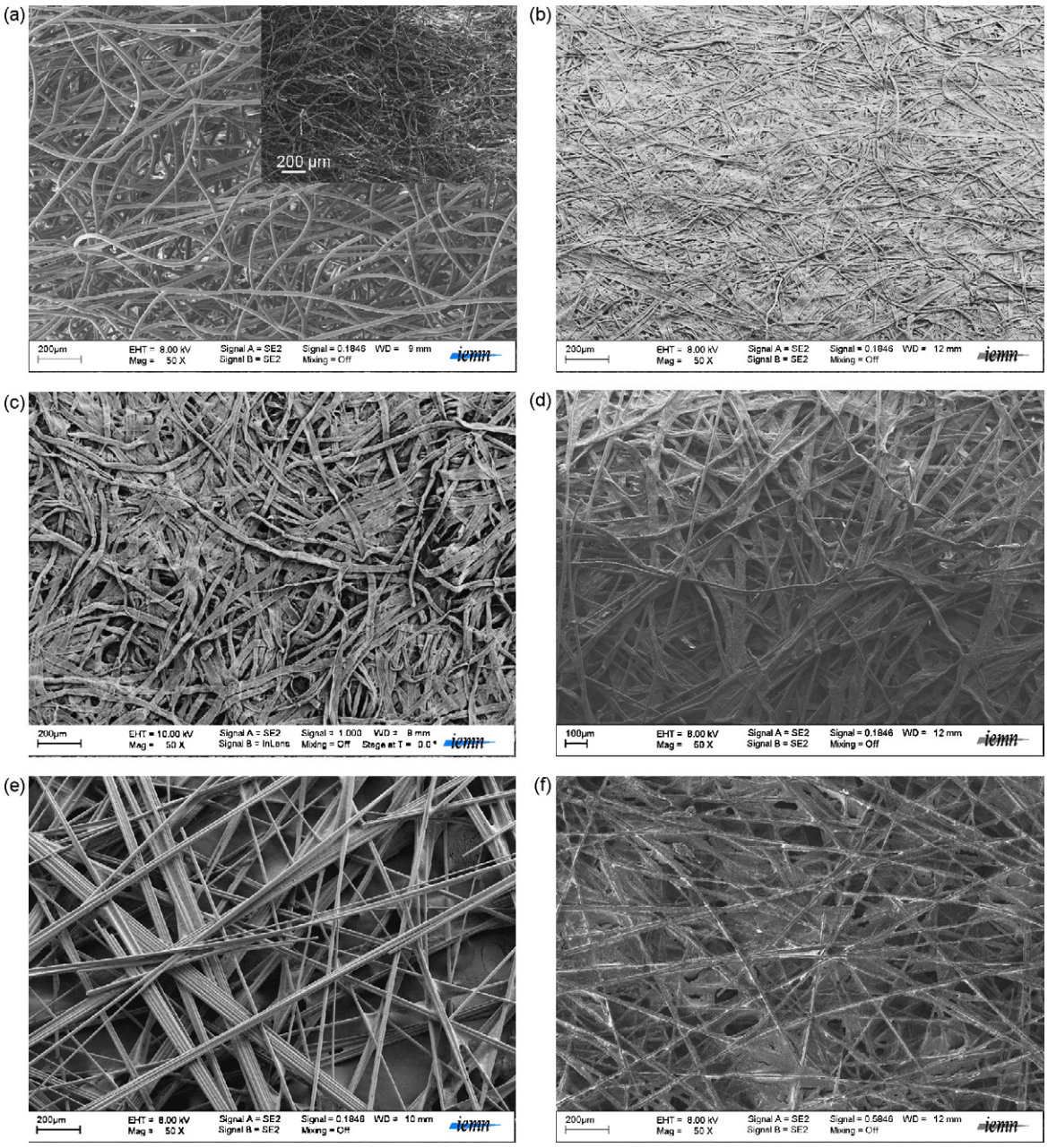

Fig. 3. (a–e) Scanning electron microscopy images of macroporous layers A–E and (f) carbon sheet; inset to (a) shows hydrophilic side of macroporous layer A.

layer(s) (light grey) having a similar thickness to the macroporous layer minimizes the compression of the macroporous layer.

In addition to the porosity, as previously stated, macroporous layer A is not symmetrical in a microfluidic sense; Fig. 5(a) shows the output power of the fuel cell with the hydrophobic surface in contact with the anode catalyst layer (configuration A1), corresponding to the previous set-up, and secondly with the hydrophilic surface in contact with the anode catalyst layer (configuration A2), see Fig. 5(b). A higher output power was observed for the second scenario; i.e. the hydrophobic surface of the macroporous layer in contact with the diffusion layer. To explain the effect of the macroporous layer at the anode we consider (i) the fuel supply distribution over the fuel cell surface and (ii) the effect of carbon dioxide bubbles exhaust. The increase in power density upon insertion of the high porosity strongly hydrophilic macroporous layer can be partly explained by the fact that the fuel performance is governed by the ability of the anode set-up (fuel flow rate, fuel concentration, microchannel dimensions, anode diffusion layer properties, e.g. porosity) to meet the anode catalyst layer's methanol requirement. Methanol concentration is known to fall along the length of the microchannel, i.e. over the surface of the cell. By inserting the high porosity hydrophilic macroporous layer between the anode diffusion layer and the anode catalyst layer one can create a fuel reservoir which leads to a more uniform methanol concentration over the whole fuel cell surface; allowing lateral flow of the fuel along the macroporous layer via capillary filling even at low fuel flow rates. As the macroporous layer has the same dimensions as the anode catalyst layer lateral fuel spreading does not occur beyond the anode catalyst layer and the fuel is localized over the active fuel cell surface.

Analytical fuel cell models given in the literature [14–18] can be very useful to predict the effect of fuel distribution along the

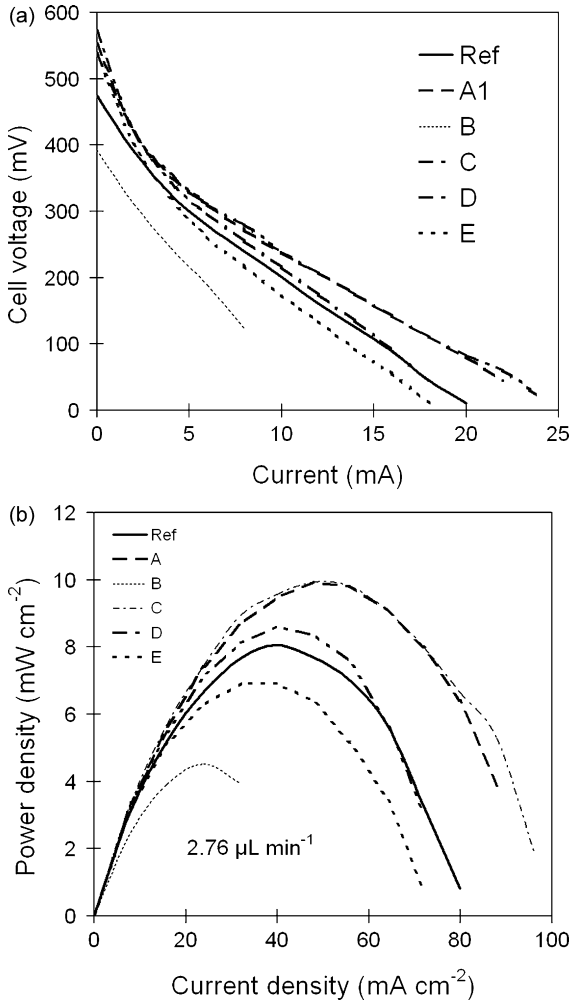

Fig. 4. Electrical measurements of the micro-DMFC after the insertion of the various macroporous layers: (a) voltage–current and (b) output power–current density.

canal in the absence of the macroporous layer. The fuel cell can be described by the following equations:

$$\frac{dc_c}{dx} = -\frac{w\Phi_d}{Q} \quad (1)$$

$$\frac{\partial c_d}{\partial z} = -\frac{\Phi_d}{D_d} \quad (2)$$

$$\Phi_m = -D_m\frac{\partial c_m}{\partial z} + \frac{\alpha J}{F} \quad (3)$$

where c_c is the methanol concentration in the x direction of the microchannel, w is the width of the microchannel, Φ_d is the methanol flux from the microchannel to the diffusion layer, Q is the input flow rate into the microchannel, c_d is the molar methanol concentration in the z direction the diffusion layer, D_d is the diffusion constant of methanol in the diffusion layer, Φ_m is the methanol crossover flux, D_m is the diffusion coefficient of methanol in the PEM, c_m is the methanol concentration across the PEM, α is the electro-osmotic drag coefficient of methanol, J is the current density and F is the Faraday constant. The models assume that there is no lateral flow in the diffusion layer and do not consider carbon dioxide production at the anode. We have implemented a multi-parameter analytical solution based on Ref. [18] which enables the determination of the methanol concentration in the anode microchannels and at the anode catalyst layer as a function of microchannel length at various anode overpotentials using the Tafel equation. The model is a relatively simple analytical model which does not take into consideration carbon dioxide generation. In as much, it generates a 'best case scenario' for the output power as a function of input fuel flow. Despite this, the model demonstrates three important predictions: (1) at the fuel flow rates used the output is a strong variation of the input fuel flow rate and (2) a low fuel flow rate (e.g. 0.55 μL min^{-1}) results in a low power output (e.g. ~1.1 mW cm^{-2}) even when carbon dioxide is not taken into account and (3) there is a power output saturation effect as a function of input fuel rate. Fig. 6(a) and (b) shows the methanol concentration at the anode catalyst layer for different input flow rates at an anode overpotential of 0.1 and 0.3 V. It is important to note here that in the absence of the macroporous layer (i) the methanol concentration falls rapidly along the microchannel especially when the overpotential is increased and (ii) the initial methanol concentration at the start of the microchannel falls with increasing anode overpotential. Fig. 6(c) shows the variation of output power density as a function of current density when the input fuel flow rate is varied from 0.55 to 8.28 μL min^{-1}. Clearly, the maximum power output is a strong variation of the input flow rate and as is observed here in the absence of the macroporous layer; c.f. Fig. 2. Fig. 6(b) also predicts (i) low output (1.1 mW cm^{-2}) for low input flow rate (0.55 μL min^{-1}) and (ii) the output power is not a linear function of the input fuel flow rate; a power output saturation effect can be expected as the input flow

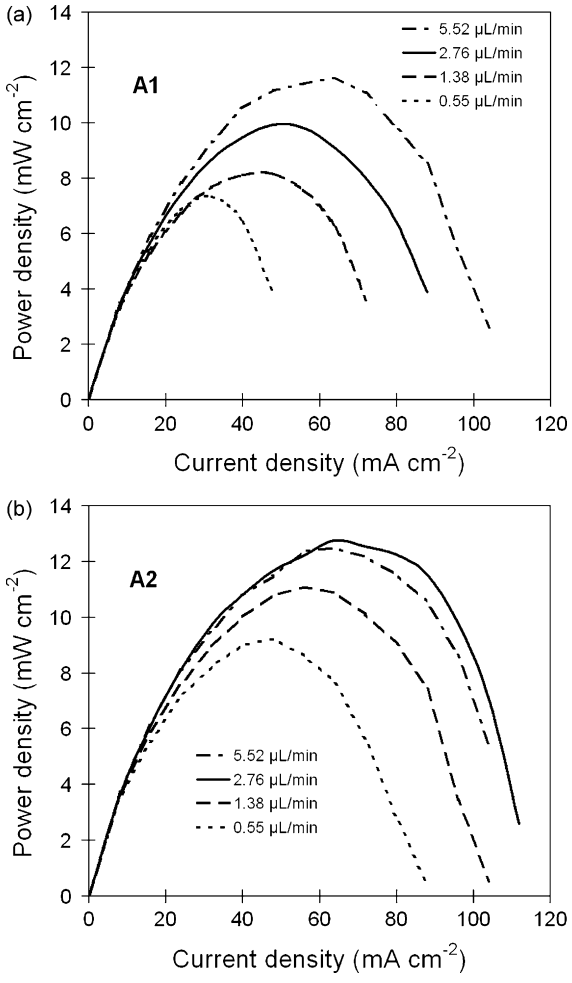

Fig. 5. (a) Output power–current density with macroporous layer A in configuration A1 (hydrophobic surface in contact with anode catalyst layer) and (b) output power–current density with macroporous layer A in configuration A2 (hydrophilic surface in contact with anode catalyst layer).

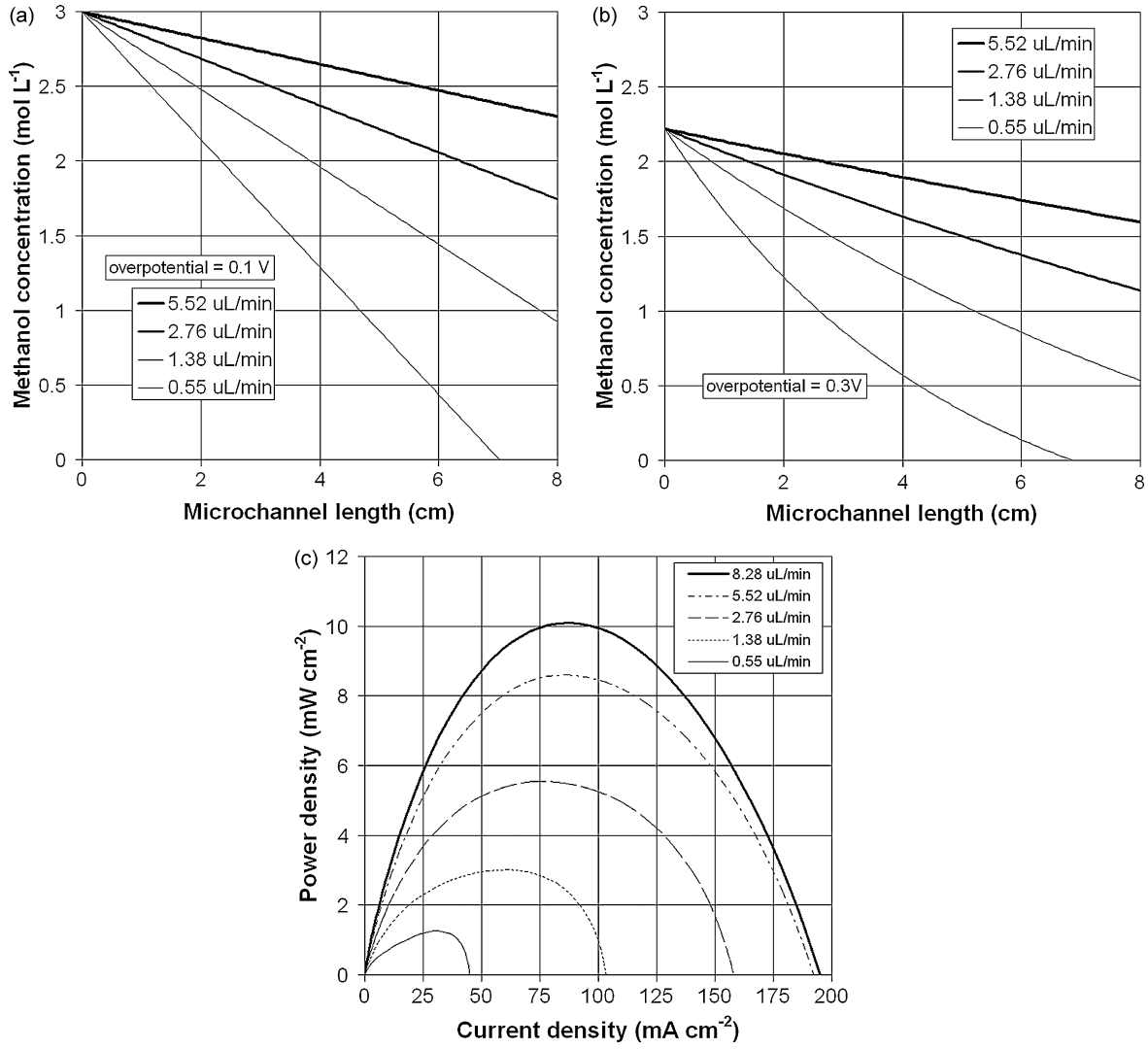

Fig. 6. Calculated methanol concentration at the anode catalyst layer at (a) anode overpotential = 0.1 V and (b) anode overpotential = 0.3 V. (c) Calculated output power–current density as a function of input fuel flow rate (at an input air-flow rate of 30 sccm to the cathode).

rate is increased; e.g. even if the input flow rate is increased beyond 10 μL min^{-1} the power output will not exceed 12 mW cm^{-2} (for a given oxygen flow rate to the cathode; 30 sccm in this case). In the absence of the macroporous layer the fuel concentration reduces along the microchannel as it is used up at the anode catalyst layer. The concentration at the anode catalyst layer reduces also with increasing microchannel length and is always less than the concentration in the microchannel directly below the diffusion layer. The insertion of a high porosity hydrophilic macroporous layer effectively leads to the possibility of a horizontal wicking of the fuel beneath the diffusion layer. In this case, a high fuel concentration at the anode catalyst layer can be maintained over the whole fuel cell surface, even at low fuel flow rates. The effect of the macroporous layer is to preserve the methanol concentration at the anode catalyst layer as the anode overpotential is increased, i.e. as methanol is being used up at the anode.

All surfaces (and we assume volumes) which were hydrophilic to the 3 M methanol/water fuel solution act as wicks and are filled by capillary action. The exception is one surface of macroporous layer A (hydrophobic to the solution) and macroporous layers D and E. This capillary filling will promote a lateral spreading of the fuel along the macroporous layer, under the diffusion layer and over the anode catalyst layer surface effectively equalizing the fuel concentration. If the porosity of the macroporous layer is very low (as is the case with macroporous layer B) then the macroporous layer can act to reduce the amount of fuel which reaches the anode catalyst layer. As the porosity of the macroporous layer is increased then fluid flow increases and lateral fluid flow via capillary filling is promoted. It is important to note that the macroporous layer must be finite and the same size as the anode catalyst layer to ensure that the fuel is localized over the anode catalyst layer otherwise the fuel would spread beyond the active surface effectively leading to fuel loss. As an analogy, the macroporous layer is acting similarly to a wick in a candle; ensuring fuel is sufficiently present for oxidation over the whole anode catalysts area much as the wick draws liquid wax to the flame via capillary action.

In addition to fuel wicking one must also consider the effect of carbon dioxide (predominantly in bubble form) at the anode [19]. Carbon dioxide bubbles must be removed from the anode catalyst layer by the anode microchannel flow. If this is not the case, carbon dioxide bubbles will build up on the anode catalyst layer and reduce the mass transport; this can be important in micro-DMFC. Theoretically in micro-direct methanol fuel cells, the detachment diameter of the carbon dioxide bubbles d_{CO_2} from the macroporous layer surface is governed by surface tension effects [20]. The value of d_{CO_2} is proportional to the pore diameter via $d_p^{1/3}$ and the wetting

Table 2
Summary of our results and modeling and comparison with values found in the literature. P_{max} = maximum output power density, J = current density at maximum output density, A = cell area, Q_{in} = input fuel flow rate, c = fuel concentration.

P_{max} (mw cm^{-2})	J at P_{max} (mA cm^{-2})	A (cm^2)	Q_{in} (μL min^{-1})	(nM s^{-1})	c (M)	Fuel use efficiency % Ref. [18]	Ref.
9.25	48	0.25	0.55	28	3	75.4	A2
11.1	56	0.25	1.38	69	3	35.1	A2
12.7	64	0.25	2.76	138	3	20.0	A2
7.36	32	0.25	0.55	28	3	50.3	A1
8.16	44	0.25	1.38	69	3	27.5	A1
9.9	50	0.25	2.76	138	3	15.6	A1
4.8	24	0.25	0.55	28	3	37.7	Ref
6.4	36	0.25	1.38	69	3	22.5	Ref
8	40	0.25	2.76	138	3	12.5	Ref
1.2	35	0.25	0.55	28	3	55	[a]
3	60	0.25	1.38	69	3	37.6	[a]
5.6	80	0.25	2.76	138	3	25	[a]
12	80	0.25	2000	16,667	0.5	0.2	[22]
14.3	80	1.6	283	4,717	1	4.7	[23]
0.29	2.5	0.25	0.166	17	6	6.5	[25]
16	75	1.625	283	9,433	2	2.2	[27]
34	150	1	800	13,333	1	1.9	[31]
9	55	0.28	2[b]	100	3	26.6	[32]
4.9	30	1	10	333	2	15.5	[35]

[a] Calculated using model.
[b] Flow rate estimated (100 μl over 50 min).

contact angle via $\sin^{1/3}\theta_c$ [20] implying that carbon dioxide bubble detachment diameter is smaller if (i) the macroporous pore diameter is smaller and (ii) the wetting contact angle of the fuel is low, i.e. the macroporous layer is hydrophilic to the fuel. Experimentally, these effects have been observed recently by Lu and Wang [8] using a transparent DMFC by comparing single layer high-pore-diameter carbon paper with a low-pore-diameter carbon cloth; they concluded that a hydrophilic layer should lead to improved carbon dioxide exhaust. We can now interpret why macroporous layer A gives a better output performance when the hydrophobic surface is in contact with the fuel diffusion layer. In this case one can predict that carbon dioxide bubble detachment will occur for smaller bubbles which can be transported away and avoid blocking and mass transport problems. When the hydrophobic layer is in contact with the anode catalyst layer, carbon dioxide bubbles will need to attain a greater diameter before detachment occurs, thus increasing mass transport issues.

In order to compare results we calculate a figure of merit, given in Eq. (4), termed fuel use efficiency φ (%) according to Ref. [21]:

$$\varphi = \frac{JA}{nFQ_{mol}} \quad (4)$$

where J is the current density (A m^{-2}) of the cell, A is the fuel cell surface area (m^2), n is the number of electrons per exchange, F is the Faraday constant (9.648×10^4 C mol^{-1}) and Q_{mol} is the molar fuel supply rate (mol s^{-1}). Our results presented here and those in the literature using silicon-based microsystems [22–35] are summarized in Table 2 where values can be extracted. It is clear that our high output power density achieved at a low fuel flow rate (0.55 μL min^{-1}) means that the calculated fuel use efficiency is high: 75.4% in the best case with the high liquid/solid volume ratio macroporous layer in configuration A1 we have a factor of 1.3 increase in the cell's fuel use efficiency compared to the reference value, i.e. without the macroporous layer and a factor of ∼2 increase in the cell's fuel use efficiency and power output for configuration A2 compared to the reference value. Table 2 can also be used to compare the model [18] and the reference data; the model predicts a higher fuel use efficiency which can be explained by the absence of carbon dioxide generation and exhaust in the model. Previous values of the fuel use efficiency [21] using silicon-based micro-direct methanol fuel cells are and 26.6% [32] and 15.5% [35] can be explained, as with our results, by the use of a low flow rate to achieve a 5–10 mW cm^{-2} output power density. Higher output power density can be achieved, e.g. ref [31], but only by using a high input fuel flow rate, as high as 800 μL min^{-1} in the case of Ref. [31], but this large fuel flow rate, >1000 times used here, leads to a reduction in the fuel use efficiency.

4. Conclusion

Microtechnology can be applied to address mass transport issues in micro-direct methanol fuel cells. We have modified the diffusion layer stack on the anode side of a micro-direct methanol fuel cell; an improved power density output is observed with the insertion of a hydrophilic macroporous layer between the standard anode diffusion layer and the anode catalyst layer compared to results obtained in the absence of this layer. The maximum power density output can be increased by a factor of ∼2; we interpret the effect of this hydrophilic macroporous layer as (i) an equalization the methanol concentration via a wicking effect over the whole anode catalyst layer surface to ensure that the methanol needs of the anode are met even at a low input flow rate and (ii) an improved carbon dioxide bubble removal rate due to the hydrophilic nature of the macroporous layer. In addition, a maximum fuel use efficiency of 75.4% is observed; this result is comparable to values found in the literature dealing with silicon-based micro-direct methanol fuel cells.

Acknowledgements

The authors would like to thank Dr. Toru Chiba and Dr. Akira Takahashi from SHARP Corporation and Professor Alain Cappy (Head of IEMN) for their support of the project.

References

[1] A.S. Arico, S. Srinivasan, V. Antonucci, Fuel Cells 1 (2001) 133–161.
[2] S.K. Kamarudin, W.R.W. Daud, S.L. Ho, U.A. Hasran, J. Power Sources 163 (2007) 743–754.
[3] E.R. Choban, L.J. Markoski, A. Wieckowski, P.J.A. Kenis, J. Power Sources 128 (2004) 54–60.
[4] A. Bazylak, D. Sinton, N. Djilali, J. Power Sources 143 (2005) 57–66.
[5] M.H. Sun, G. Velve Casquillas, S.S. Guo, J. Shi, H. Ji, Q. Ouyang, Y. Chen, Microelectron. Eng. 84 (2007) 1182–1185.

[6] A. Heinzel, V.M. Barragán, J. Power Sources 84 (1999) 70–74.
[7] B. Gurau, E.S. Smotkin, J. Power Sources 112 (2002) 339–352.
[8] G.Q. Lu, C.Y. Wang, J. Power Sources 134 (2004) 33–40.
[9] M.D. Lundin, M.J. McCready, J. Power Sources 172 (2007) 553–559.
[10] C. Litterst, S. Eccarius, C. Hebling, R. Zengerle, P. Koltay, J. Micromech. Microeng. 16 (2006) S248–S253.
[11] K. Scott, W.M. Taama, P. Argyropoulos, K. Sundmacher, J. Power Sources 83 (1999) 204–216.
[12] T. Schultz, K. Sundmacher, J. Membr. Sci. 276 (2006) 272–285.
[13] G. Jewett, Z. Guo, A. Faghri, J. Power Sources 168 (2007) 434–446.
[14] P. Argyropoulos, K. Scott, A.K. Shukla, C. Jackson, J. Power Sources 123 (2003) 190–199.
[15] B.L. García, V.A. Sethuraman, J.W. Weidner, R.E. White, R. Dougal, J. Fuel Cell Sci. Technol. 1 (2004) 43–48.
[16] R. Chen, T.S. Zhao, J. Power Sources 152 (2005) 122–130.
[17] K. Scott, C. Jackson, P. Argyropoulos, J. Power Sources 161 (2006) 885–892.
[18] H. Guo, C.-F. Ma, Electrochem. Commun. 6 (2004) 306–312.
[19] K. Scott, W.M. Taama, P. Argyropoulos, Electrochim. Acta 44 (1999) 3575–3584.
[20] G.B. Wallis, One Dimensional Two-phase Flow, McGraw-Hill, New York, 1969.
[21] R. O'Hayre, S.-W. Cha, W. Colelle, F.B. Prinz, Fuel Cell Fundamentals, John Wiley & Sons, New York, 2006.
[22] S.C. Kelley, G.A. Deluga, W.H. Smyrl, Electrochem. Solid-State Lett. 3 (2000) 407–409.
[23] T.J. Yen, N. Fang, X. Zhang, G.Q. Lu, C.Y. Wang, Appl. Phys. Lett. 83 (2003) 4056–4058.
[24] Y.H. Seo, Y.H. Cho, Proceedings of the 16th Annual International Conference on Micro Electro Mechanical Systems, IEEE, MEMS-03, Kyoto, 2003, pp. 375–378.
[25] K. Wozniak, D. Johansson, M. Bring, A. Sanz-Velasco, P. Enoksson, J. Micromech. Microeng. 14 (2004) S59–S63.
[26] S. Motokawa, M. Mohamedi, T. Momma, S. Shoji, T. Osaka, Electrochem. Commun. 6 (2004) 562–565.
[27] G.Q. Lu, C.Y. Wang, T.J. Yen, X. Zhang, Electrochim. Acta 49 (2004) 821–828.
[28] J. Yeom, G.Z. Mozsgai, B.R. Flachsbart, E.R. Choban, A. Asthana, M.A. Shannon, P.J.A. Kenis, Sens. Actuators B 107 (2005) 882–891.
[29] S.-C. Yao, X. Tang, C.-C. Hsieh, Y. Alyousef, M. Vladimer, G.K. Fedder, C.H. Amon, Energy 31 (2006) 636–649.
[30] Y. Jiang, X. Wang, L. Zhong, L. Liu, J. Micromech. Microeng. 16 (2006) S233–S239.
[31] C.W. Wong, T.S. Zhao, Q. Ye, J.G. Liu, J. Power Sources 155 (2005) 291–296.
[32] J.P. Esquivel, N. Sabate, J. Santander, N. Torres, C. Cane, Microsyst. Technol. 14 (2008) 535–541.
[33] Y. Zhang, J. Lu, S. Shimano, H. Zhou, R. Maeda, Electrochem. Commun. 9 (2007) 1365–1368.
[34] Q. Zhang, X. Wang, L. Zhong, Y. Zhou, X. Qiu, L. S Liu, Proceedings of the MEMS, Tucson, AZ, USA, 2008, pp. 972–975.
[35] X. Liu, C. Suo, Y. Zhang, X. Wang, C. Sun, L. Li, L. Zhang, J. Micromech. Microeng. 16 (2006) S226–S232.